Stanford Exploration Project, Report 97, July 8, 1998, pages 83–95

Stanford Exploration Project, Report 97, July 8, 1998, pages 83–95

Azimuth moveout vs. dip moveout in inhomogeneous media

Biondo L. Biondi[1]

keywords: *AMO, DMO*

ABSTRACT

Dip moveout (DMO) is often applied to prestack data to better preserve dipping events when performing partial stacks over ranges of offset. The tests presented in this paper, conducted on the SEG-EAGE salt data set, indicate that the application of azimuth moveout (AMO) in place of constant-velocity DMO yields better partial stacks in two important cases: first, when the velocity increases with depth. Second, when a salt body causes NMO-velocity conflicts between deeper flat reflectors and shallower dipping reflectors.
AMO is less sensitive to velocity variations than DMO because it is a residual operator, and thus it has less tendency to overcorrect reflections that have been moved out with too high NMO velocity. AMO has also the potential advantage over $V(z)$ DMOs to be less sensitive to the given velocity function.

INTRODUCTION

Dip moveout (DMO) is being used today for a wider range of applications than its original target of transforming prestack data to zero-offset before global (i.e. over the whole offset axis) stacking and zero-offset migration. An increasingly popular application of DMO is to improve the accuracy of stacking the data over a limited range offsets. This partial-stacking procedure can be used to reduce the cost of prestack imaging both in time (Ferber et al., 1996) and depth (Canning and Gardner, 1996; Biondi, 1997). The application of DMO before partial stacking improves the coherency of the stack of dipping events.

The main motivation for applying partial stacking instead of global stacking is to improve the final image when the velocity function does not fulfill the simple assumptions at the basis of the conventional normal moveout (NMO) and DMO process. After partial stacking the data size is considerably reduced, but the results are still segregated by offset ranges. Usually the output of partial stacking is organized in

[1]**email:** biondo@sep.stanford.edu

pseudo common-offset cubes, that can be imaged in several ways. For time-imaging purposes, one common procedure is to apply zero-offset migration to each pseudo common-offset cube and then apply a residual NMO correction before stacking (Ferber et al., 1996). Another common practice is to transform the *pseudo* common-offset cubes into *true* common-offset cubes by inverse DMO (Ronen, 1987; Canning and Gardner, 1996). These common-offset cubes can then be imaged by a full prestack depth migration or prestack time migration. Other than to reduce the cost of prestack migration for structural imaging, partial stacking after DMO is also commonly used for AVO analysis, specially in the Gulf of Mexico. The AVO trend is usually measured from the common-offset cubes after migration has focused the diffractions and correctly positioned the amplitude anomalies.

The accuracy of partial stacking after DMO depends on the degree of velocity variations in the subsurface, both vertical and lateral. For partial stacking to enhance reflections and suppress noise, reflections need to be coherent across the traces to be stacked. Hale and Artley (1993) and Hawkins et al. (1995) showed that even in a simple vertically layered medium constant-velocity DMO is not accurate in correcting the kinematics of dipping reflectors. Although partial stacking is less sensitive than global stacking to velocity variations because the offset range is narrower, nevertheless it is not compleatly insensitive. The accuracy of the partial stacking process is particularly important for AVO applications. Uncoherent stacking caused by small relative shifts between the traces is sufficient to alter the AVO response of dipping events (Rietveld et al., 1997).

Partial stacking after azimuth moveout (AMO) is an alternative to partial stacking after DMO. Biondi et al. (1998) defined AMO as the operator that is equivalent to the the chain of DMO followed by inverse DMO. In this paper I demonstrate that, when the velocity increases with depth, partial stacking after AMO is more accurate than partial stacking after constant-velocity DMO. I also show an example in which partial stacking after AMO is less sensitive than partial stacking after constant-velocity DMO to a large lateral increase in the NMO velocity function. Although AMO and DMO are strictly related, the two processes that I compare yield different results because the domains in which the data are partially stacked are different. The data are stacked in the zero-offset domain after DMO, but the data are stacked in the finite-offset domain after AMO. AMO has the intrinsic advantage over DMO to be only a residual transformation. It transforms the data from one finite offset to a nearby finite offset; in contrast, DMO transforms the data all the way to zero offset. Therefore, the AMO operator moves the dipping events along the midpoint directions less than the DMO operator does, and it is consequently less sensitive to deviations from the underlying assumption of constant velocity.

Several authors presented generalizations of DMO to depth-variable velocity functions (Popovici, 1990; Perkins and French, 1990; Hale and Artley, 1993; Dietrich and Cohen, 1993; Meinardus and Schleicher, 1993; Hawkins et al., 1995; Sun and Alkhalifah, 1998); these $V(z)$ DMOs could be used in place of constant-velocity DMO to improve the accuracy of partial stacking. One important drawback of $V(z)$ DMOs is

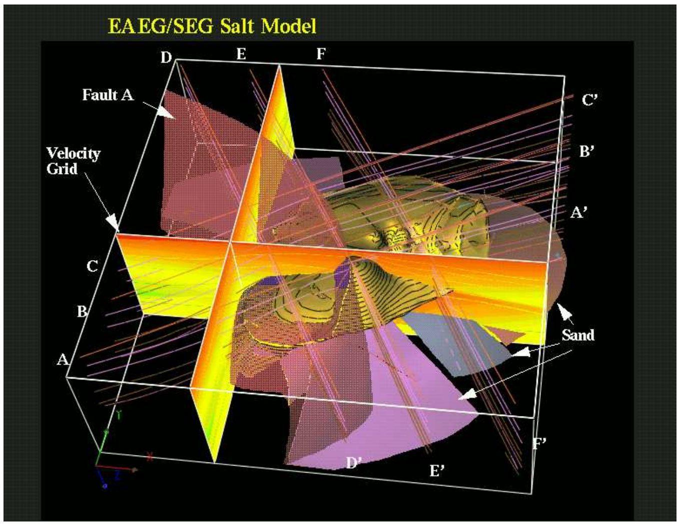

Figure 1: 3-D representation of the SEG-EAGE salt model. biondo1-salt [NR]

that they are quite sensitive to the accuracy of the input velocity function. Another drawback is that the $V(z)$-DMO operators often have cusps and triplications. These singularities make the implementation of $V(z)$ DMO as integral operators prone to artifacts and/or computationally intensive. Because it is a residual operator, AMO is spatially compact and inexpensive to apply. The impulse response is a skewed saddle and is single valued, though its implementation as integral operator requires some care (Biondi et al., 1998). A $V(z)$ AMO operator can also be derived by cascading $V(z)$ DMO with its inverse (Alkhalifah and Biondi, 1998). Alkhalifah and Biondi (1998) show that, whereas the $V(z)$ AMO operator may have triplications, it in general a better behaved operator than the $V(z)$ DMO operator.

Furthermore, to my knowledge, no implementation of inverse $V(z)$ DMO has been presented in the literature yet. Therefore, some of the most advanced uses of DMO coupled with inverse DMO, such as prestack depth migration after partial stacking (Biondi, 1997; Mosher et al., 1997), and spatial dealiasing (Ronen, 1987; Brink et al., 1997) cannot exploit the improved accuracy of $V(z)$ DMO.

In this paper I will only show the results of comparing partial stacking after DMO and AMO; Biondi et al. (1998) developed the theory of AMO. For my tests, I use the subset of the SEG/EAGE salt data set (Aminzadeh et al., 1996) known as C3 Narrow-Azimuth classic data set (C3-NA) (1997). The data were recorded on the realistic and complex salt-dome structure shown in Figure 1.

TESTS ON THE SEG/EAGE SALT DATA SET

The Salt Model C3-NA data set simulates a narrow-azimuth marine acquisition with 8 streamers recorded on an area about one quarter of the whole model. The maximum absolute offset is about 2,600 m and the maximum cross-line offset between the sources and the outer streamers is ±140 m. The in-line direction is East-West,

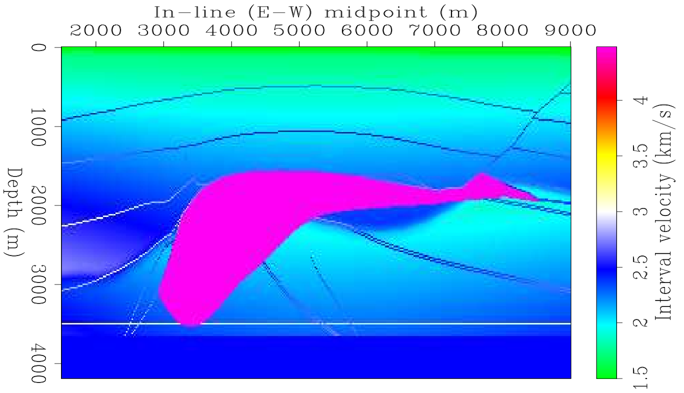

Figure 2: In-line vertical section through the interval velocity model. biondo1-Vel-sec [CR]

corresponding to the approximate North-South direction in the model as displayed in Figure 1. Notice that the Figure displays the model rotated with respect to its "true" orientation; that is, the "true North" of the model points to the West of the Figure.

The fault plane indicated as "Fault A" in Figure 1 is a good reflector for testing methods of partial stacking, in particular where it cuts through the salt body and creates a high-reflectivity interface between the top of the salt and the sediments above. Figure 2 shows an example of in-line section through the velocity model. In this section "Fault A" is in the top-right corner; the shallower part of the fault cuts through sediments, while the deeper part coincides with the top of the salt. The section in Figure 2 is approximately located as the in-line vertical section displayed in Figure 1. Notice that the vertical/horizontal aspect ratio is not preserved in Figure 2 and thus the fault appears to be dipping at a steeper angle with respect to the in-line direction than its true dip of about 40°.

At the North-East corner of the recording area the reflections from the fault-plane are free from interferences with the salt body, and thus can be used for comparing DMO and AMO in a horizontally layered medium. However, towards the center of the model the fault-plane reflections move rapidly under the "shadow" of the salt body, and therefore they are useful for comparing the sensitivity of DMO and AMO to NMO-velocity conflicts.

The tests compare the results of three methods for transforming prestack data after NMO and before partial stacking: a) simple binning with spatial interpolation, b) AMO and c) DMO. All the data within the 2–2.5 km offset range were transformed using these three methods. No inverse NMO was applied after the transformation. To enable the analysis of the moveouts along the offset axis after the application of DMO and AMO, the results are organized in pseudo-offset cubes with a narrow-offset ranges of 100 m.

The AMO and DMO operators have similar implementations. They use the same anti-aliasing method and the same temporal and spatial interpolations. For the test data set, the computational times were also comparable. By optimizing the spatial

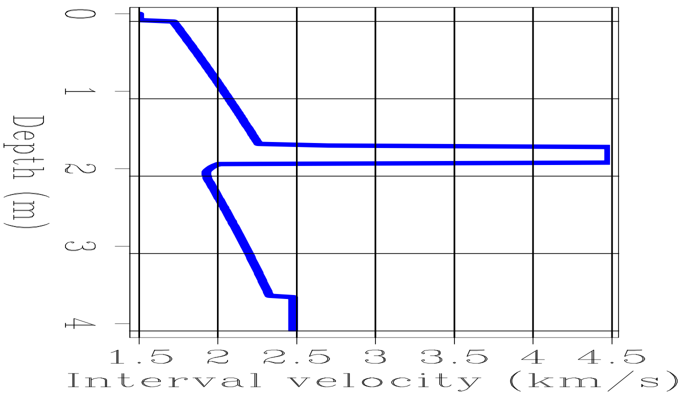

Figure 3: Typical vertical velocity profile in the area of study. biondo1-Vel-1D [CR]

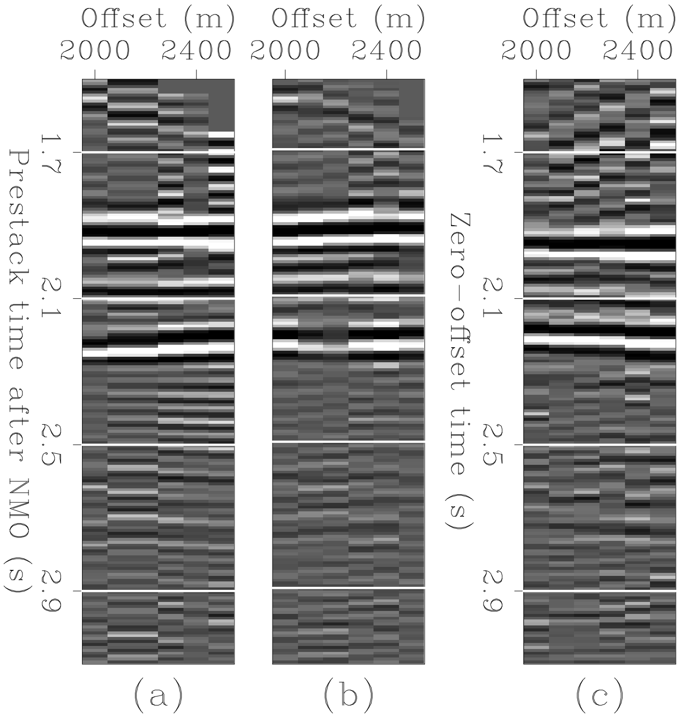

Figure 4: CMP gathers after NMO and the application of: (a) Binning, (b) AMO, and (c) DMO. The fault-plane reflection is at about 2.2 s. biondo1-All-XYs [CR]

sampling of the AMO operator, it should be possible to obtain an even faster, but as accurate, AMO implementation (Biondi et al., 1998).

Vertical velocity gradient

Figure 3 shows the velocity as a function of depth at one surface location in the area where the salt body does not interfere with the fault reflections. Although the velocity gradient of about 0.4 s^{-1} is relatively mild in absolute terms, it is the strongest within this salt model. The effects of the vertical gradient on the moveouts of the reflections after DMO and AMO are measurable, but not too strong. Figure 4 shows the moveouts of the reflection from the fault at a typical CMP location in the area. As expected, the moveout after simple binning (a) points upward with offset, because of the dip effect. Also not surprisingly, the moveout after DMO (c) points downward with offset. Hale and Artley (1993), and several others authors, showed that constant-velocity DMO overcorrects the moveouts in a horizontally layered medium with velocity increasing with depth. In contrast, the moveout from the fault reflection is approximately flat after AMO (b). The simple explanation of these results is that AMO is a residual operator and consequently moves energy less than DMO does. Therefore, it overcorrects the moveout less than constant velocity DMO. In some respects, it behaves similarly to the "squeezed DMO" presented by Hale and Artley (1993).

NMO-velocity conflict

The fault-plane reflections for the CMP shown in Figure 4 are free from interferences with the salt body. But these events move quickly under the "shadow" of the salt body as the CMP location moves towards the middle of the model. In this area, the fault-plane reflections are still propagating in the sediments, but they are recorded at surface locations that are right above the salt, and at traveltimes larger than the two-way vertical traveltime from both the top and the bottom of the salt. This situation creates a conflict between the NMO velocity that is correct for the flatter events (e.g. top and bottom of the salt) and the NMO velocity that is correct for the fault-plane reflections. This kind of NMO-velocity conflict creates problems for constant-velocity DMO, that has the tendency to overcorrect the moveout of the dipping events, as discussed by several authors (Meinardus and Schleicher, 1993; Hawkins et al., 1995; Rietveld et al., 1997).

Figure 5 shows a time-slice of the root-mean-square (RMS) velocity computed from the interval velocity model. This time slice is cut at approximately the traveltime of the fault-plane reflection for the 2–2.5 km offset range. The fault plane cuts this time slice from the top-left corner (at a cross-line midpoint of about 4 km) to the bottom middle (at a cross-line midpoint of about 7 km). Figure 6, Figure 7, and Figure 8 show the effects of the NMO-velocity conflict on the partial stacking of the fault-plane reflections. The Figures show time-slices of the result of partial stacking the data over the whole 2–2.5 km offset range after the application of: binning (Figure 6), AMO (Figure 7), and DMO (Figure 8). The fault reflections below the salt, (labeled as "below" salt in the Figures) are wiped out by partial stacking after DMO. In contrast, they are reasonably well preserved after either binning or AMO. However, the salt-flanks reflections that are not affected by the NMO-velocity conflict (labeled as "above" salt in the Figures) are strongly attenuated after binning, and well preserved after either DMO or AMO. In summary, AMO well preserves all the dipping events, irrespective whether they are "below" or "above" the salt. In contrast, both binning and DMO attenuate one of the two types of dipping events. The explanation of these results is similar to the explanation of the results obtained in the horizontally layered part of the model. AMO applies a smaller correction to the data than DMO does, and thus AMO does not overcorrect data that have been moved out with a too fast NMO velocity. But AMO also properly corrects the data that are not in the shadow of the salt body and have been moved out with the appropriate NMO velocity.

Similar results are obtained when the same experiment is carried out for the mid-offset range (1.2–2.0 km). Figure 9-11 show the results of partial stacking over the whole offset range after the application of: binning (Figure 9), AMO (Figure 10), and DMO (Figure 11). The fault reflections and some of the slat-flanks reflections that are "below" the salt are severely affected by partial stacking after DMO. In contrast, they are reasonably well preserved after either binning or AMO. Notice, however, that the steeply dipping salt-flank reflections (at an in-line midpoint location of about 7 km) are better preserved after AMO than after simple binning.

CONCLUSIONS

The results of the tests presented in this paper indicate that, when the velocity function increases with depth or there are NMO-velocity conflicts, AMO is a more robust process than constant-velocity DMO to transform prestack data before performing partial stacks. AMO performs better than constant-velocity DMO because it is a residual operator, and thus does not overcorrect data that have been moved out with a too fast NMO velocity.

The results of these tests encourage further comparison of AMO with $V(z)$ DMOs, and possibly in data sets collected in areas where transverse anisotropy plays an important role.

REFERENCES

Alkhalifah, T., and Biondi, B., 1998, The azimuth moveout operator for vertically inhomogenous media: SEP–**97**, 95–116.

Aminzadeh, F., Burkhard, N., Long, J., Kunz, T., and Duclos, P., 1996, Three dimensional SEG/EAEG models - an update: The Leading Edge, **2**, 131–134.

Biondi, B., Fomel, S., and Chemingui, N., 1998, Azimuth moveout for 3-D prestack imaging: Geophysics, **63**, no. 2, 574–588.

Biondi, B., 1997, Azimuth moveout + coomon-azimuth migration: Cost-effective prestack depth imaging of marine data: 67th Annual Internat. Mtg., Soc. Expl. Geophys., Expanded Abstracts, 1375–1378.

Brink, M., Gimse, I., Turner, P., Stolte, C., and Ronen, S., 1997, Resolution and coverage beyond traditional limits: 67th Annual Internat. Mtg., Soc. Expl. Geophys., Expanded Abstracts, 1123–1127.

Canning, A., and Gardner, G. H. F., 1996, Regularizing 3-D data sets with DMO: Geophysics, **61**, 1103–1114.

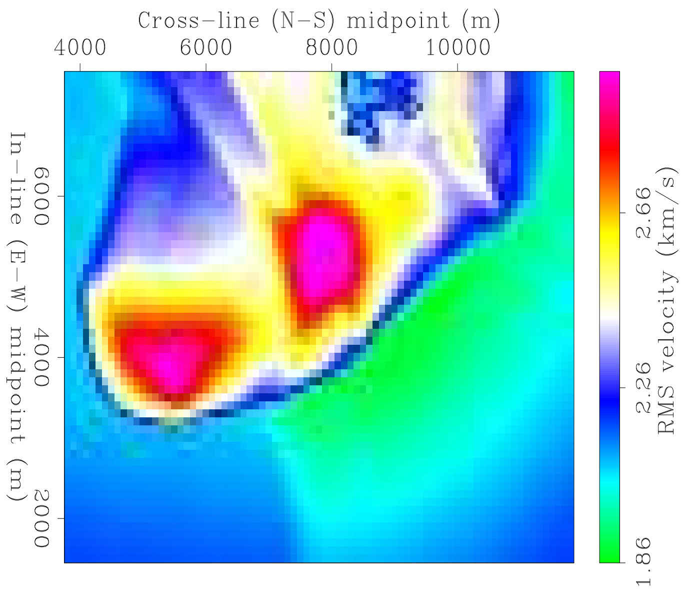

Figure 5: Time slice through the RMS velocity function, taken at the same traveltime of the time slices shown in Figure 6, 7, and 8. biondo1-Vel-rms [CR]

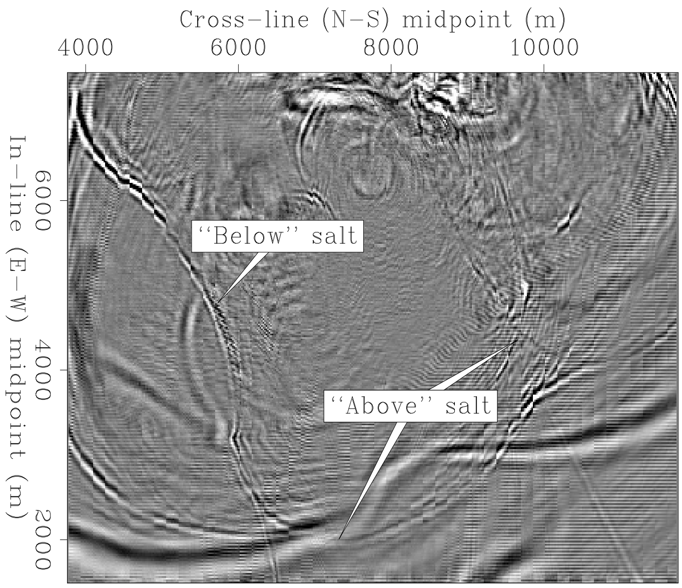

Figure 6: Time slice through the results of partial stacking the far-offset range (2–2.5 km) after binning. The "above"-salt reflections are strongly attenuated. biondo1-Ts-Bin-stack-box [CR]

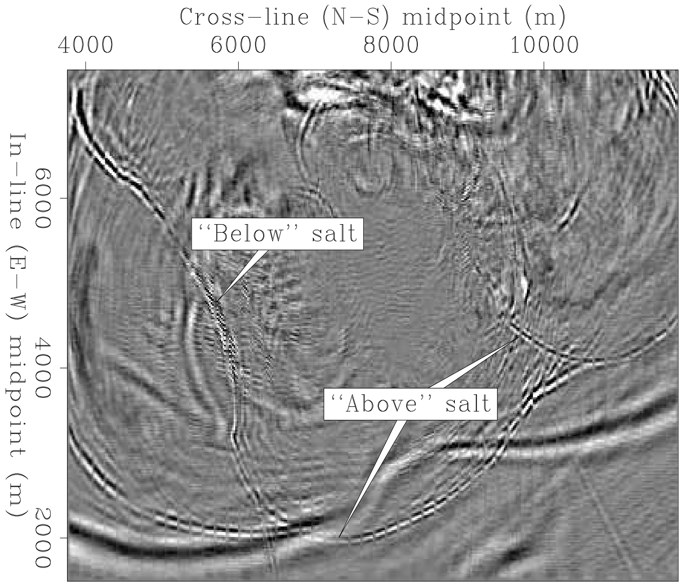

Figure 7: Time slice through the results of partial stacking the far-offset range (2–2.5 km) after AMO. Reflections from "below" and "above" the salt are both well preserved. biondo1-Ts-Amo-df-stack-box [CR]

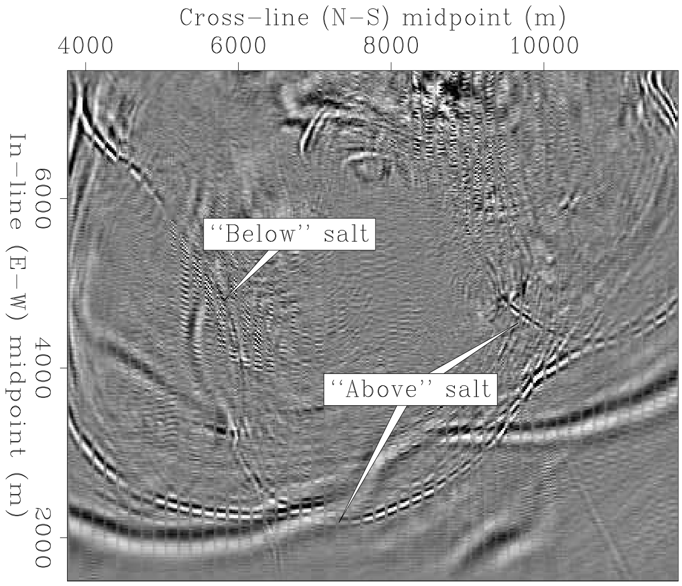

Figure 8: Time slice through the results of partial stacking the far-offset range (2–2.5 km) after DMO. The "below"-salt reflections are strongly attenuated. biondo1-Ts-Dmo-df-stack-box [CR]

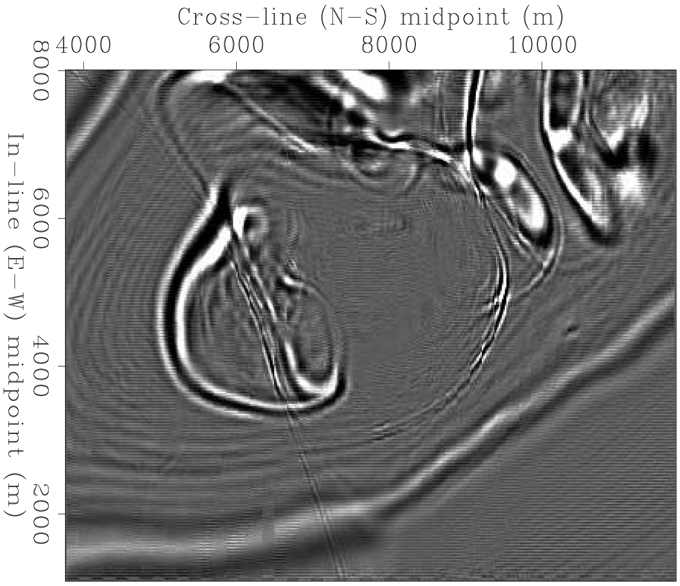

Figure 9: Time slice through the results of partial stacking the mid-offset range (1.2–2 km) after binning. biondo1-Ts-Bin-2 [CR]

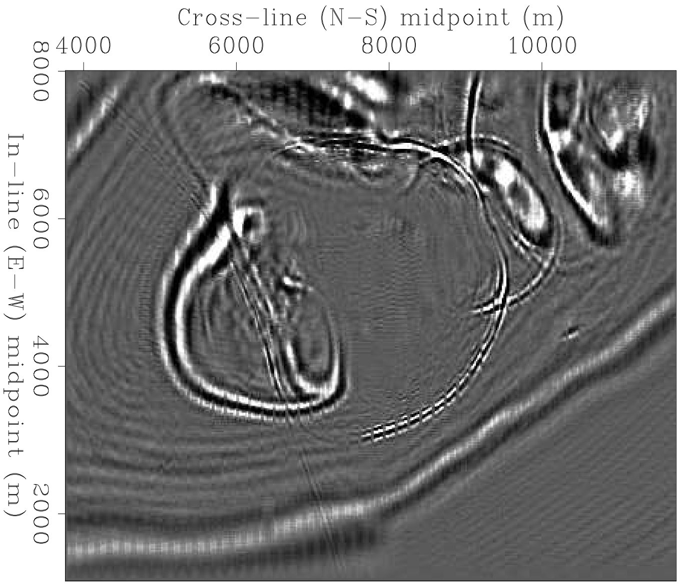

Figure 10: Time slice through the results of partial stacking the mid-offset range (1.2–2 km) after AMO. biondo1-Ts-Amo-df-2 [CR]

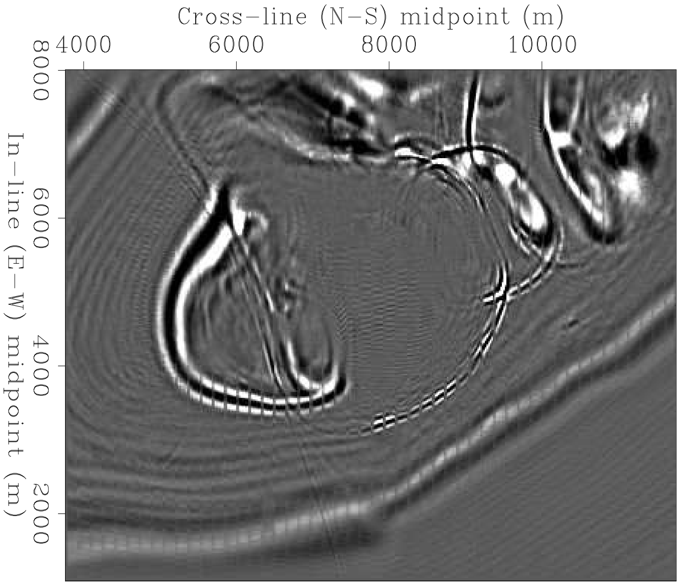

Figure 11: Time slice through the results of partial stacking the mid-offset range (1.2–2 km) after DMO. biondo1-Ts-Dmo-df-2 [CR]

Dietrich, M., and Cohen, J. K., 1993, Migration to zero offset (DMO) for a constant velocity gradient: An analytical formulation: Geophys. Prosp., **41**, no. 5, 621–644.

Ferber, R., Sanders, B., and Yilmaz, O., 1996, Quick-look 3-D prestack time migration: 65th Annual Internat. Mtg., Soc. Expl. Geophys., Expanded Abstracts, 451–454.

Hale, D., and Artley, C., 1993, Squeezing dip moveout for depth-variable velocity: Geophysics, **58**, 257–264.

Hawkins, K., Cheng, C. C., Sadek, S. A., and Brzostowski, M. A., 1995, A v(z) DMO developed with the north sea central graben in mind: 65th Annual Internat. Mtg., Soc. Expl. Geophys., Expanded Abstracts, 1429–1432.

Meinardus, H. A., and Schleicher, K. L., 1993, 3-D time-variant dip moveout by the f-k method: Geophysics, **7**, 1030–1041.

Mosher, C. C., Foster, D. J., and Hassanzadeh, S., 1997, Common angle imaging with offset plane waves: 67th Annual Internat. Mtg., Soc. Expl. Geophys., Expanded Abstracts, 1379–1382.

Perkins, W. T., and French, W. S., 1990, 3-D migration to zero offset for a constant velocity gradient: 60th Annual Internat. Mtg., Soc. Expl. Geophys., Expanded Abstracts, 1354–1357.

Popovici, A. M., 1990, Kinematics of prestack partial migration in variable velocity media: 60th Annual Internat. Mtg., Soc. Expl. Geophys., Expanded Abstracts, 1337–1341.

Rietveld, W. E. A., Marfurt, K. J., and Kommedal, J. H., 1997, The effect of 3-D prestack seismic migration on seismic attrubute analysis: 67th Annual Internat. Mtg., Soc. Expl. Geophys., Expanded Abstracts, 1367–1370.

Ronen, J., 1987, Wave-equation trace interpolation: Geophysics, **52**, no. 7, 973–984.

SEG-EAGE, 1997, Salt Model Narrow-Azimuth Classic dataset (C3-NA): http://archive.llnl.gov/SSD/classic/classicSalt.html#salt-c.

Sun, Y., and Alkhalifah, T., 1998, Building the 3-D integral DMO operator in the slant-stack domain: 68th Annual Internat. Mtg., Soc. Expl. Geophys., Expanded Abstracts, submitted.